Theoretical Analysis of Time-Dependence and Thixotropy of Fluidity for High Fluidity Concrete

Zhuguo Li[1]; Taka-aki Ohkubo[2]; and Yasuo Tanigawa[3]

Abstract: This paper deals with the time dependence of fluidity and thixotropy of high fluidity concrete containing polycarboxylate-based superplasticizer. Taking the effects of both hydration and physical flocculation of cement particles into consideration, the increases in apparent viscosity and Bingham constants with the elapsed time of the stationary state, and the time dependence of the apparent viscosity in agitated state, are theoretically investigated. Moreover, the effects of the number, peak value, and durations of applied stepwise stresses, etc., on the shape and the area surrounded by the hysteresis loop of shear rate versus shear stress are discussed quantitatively.

DOI: 10.1061/(ASCE)0899-1561(2004)16:3(247)

CE Database subject headings: Concrete; Time dependence; Material properties; Shear stress; Flocculation; Hydration.

Introduction

High fluidity concrete can be cast without compaction. However, whether or not it has the required self-compaction characteristics when it is cast depends not only on its fluidity immediately after mixing, but also on the maintenance of its fluidity until casting. Investigations on the rheological properties of high fluidity concrete have previously concentrated on methods of test and evaluation of its consistency, and the factors influencing its consistency, including mainly the properties of raw materials used and their mix proportions, etc. (e.g., JCI 1993; JCSE 1996). A standard rheological test method has not yet been established for fresh concrete, and material characteristics may lack stability due to segregation during testing. These factors make it hard to perform precise experimental investigations on the rheology of fresh concrete. As a result, some experiments have also been conducted on the time dependence of rheological behaviors (standstill time or agitation time), e.g., slump flow loss and thixotropy (Hu et al. 1996; Masuda et al. 1998; Billerg and Osterberg 2001; Toussaint et al. 2001), but an overall understanding and quantification are yet far from being achieved.

Since a lot of high fluidity concrete is produced using a polycarboxylate-based superplasticizer, this study first aims to clarify the time dependence of fluidity and thixotropic characteristic of this type of high fluidity concrete. Using a theoretical approach and numerical analysis, investigations are made on the variations of the apparent viscosity or Bingham's constants with standstill or agitation time, and the shape and area surrounded by the hysteresis loop of shear rate–stepwise shear stress relationship curve.

[1]Domestic Research Fellow, Dept. of Building Materials and Components, Building Research Institute, 1-Tachihara, Tsukuba, Ibaraki 305-0802, Japan. E-mail: lizhuguo@hotmail.com

[2]Chief Research Engineer, Dept. of Building Materials and Components, Building Research Institute, 1-Tachihara, Tsukuba, Ibaraki 305-0802, Japan.

[3]Professor, Division of Environmental Engineering and Architecture, Graduate School of Environmental Studies, Nagoya Univ., Chikusa-ku, Nagoya 464-8603, Japan.

Note. Associate Editor: Manoochehr Zoghi. Discussion open until November 1, 2004. Separate discussions must be submitted for individual papers. To extend the closing date by one month, a written request must be filed with the ASCE Managing Editor. The manuscript for this paper was submitted for review and possible publication on October 22, 2002; approved on March 24, 2003. This paper is part of the ***Journal of Materials in Civil Engineering***, Vol. 16, No. 3, June 1, 2004. ©ASCE, ISSN 0899-1561/2004/3-247–256/$18.00.

Shear Rate and Apparent Viscosity

According to the past study of one of the writers (Li 2001), high fluidity concrete can be considered as a kind of particle assembly composed of adhesive particles (cement grains) whose displacement is time dependent, and cohesionless particles (aggregates grains) whose displacement is time independent. The angle included between the contact plane of particle and the maximum shear plane is referred to as particle contact angle. When the mean particle contact angle of the particle assembly is approximated as zero, the flow curve of high fluidity concrete, as shown as in Fig. 1, the shear rate ($\dot{\gamma}$), and the apparent viscosity (η_a), which is the ratio of shear stress (τ) to shear rate, are, respectively, expressed as

$$\dot{\gamma} = C_1 \exp\left(-\frac{E}{kT}\right) \sinh[C_2(\tau - \tau_y)] \tag{1}$$

$$\eta_a = \frac{\tau}{C_1} \exp\left(\frac{E}{kT}\right) \frac{1}{\sinh[C_2(\tau - \tau_y)]} \tag{2}$$

where $C_1 = 2kT/hN_c\Lambda_{cm}$; $C_2 = S_d\Lambda_{cm}/2kTN_c$; E = mean potential energy of one cement particle that creates a viscous resistance to cement particle movement; N_c = number of cement particles per unit dimension; Λ_{cm} = mean distance of cement particle movement when fresh concrete flows; k = Boltzmann's constant; h = Planck's constant; T = absolute temperature; and S_d = stress distribution coefficient that is equal to a ratio of the volume of cement particles to the total volume of all solid particles in unit concrete (Li et al. 2002).

The τ_y in Eq. (1), which is referred to as the true yield stress of fresh high-fluidity concrete, i.e., a shear stress supported by inter-frictional resistance in fresh concrete, is given by (Li et al. 2002)

$$\tau_y = \sigma_n \tan\phi_m + C_w \tag{3}$$

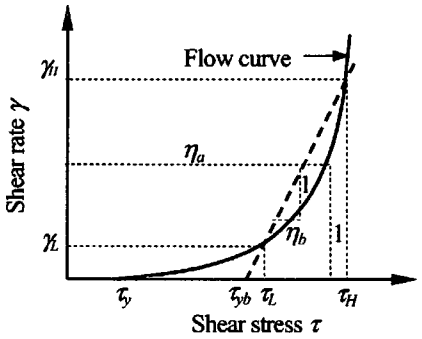

Fig. 1. Apparent viscosity and Bingham constants of fresh concrete

where σ_n = normal stress on the shear plane; ϕ_m = mean interfrictional angle of the particle assembly; and C_w = constant that is referred to as an increase in the shear resistance of fresh concrete caused by the surface tension of the mixing water.

When producing high fluidity concrete by mixing polycarboxylate-based superplasticizer, the repulsive interaction between cement particles mainly results from steric hindrances of polymers absorbed onto the cement particle surfaces (Sakai and Daimonn 1996). This steric hindrance effect is composed of an elastic term and a mixing term, which depend on the thickness and the density, respectively, of the polymer adsorption layer. The mixing term is due to a resistance occurring when the neighboring polymer layers invade each other, but the elastic term is a repulsive force from the polymer chains when neighboring cement particles come close to each other. Because the thickness (δ) of the polymer adsorption layer depends on the structural character of the polymer (Everett et al. 2000), for a given variety of polycarboxylate-based superplasticizer, δ is a constant of that polymer. Due to the elastic term of the steric hindrance, two cement particles that have absorbed the polymers can come close to each other only at a certain position beyond the polymer absorption layers. The intercement potential energy curve is indicated by curve (i) or (ii) in Fig. 2. The stable stop position corresponds to the inflection point (hereafter called the minimum point) on the potential energy curve, which is in the range of δ–2δ. Thus, the potential energy of the cement particle that has absorbed the polymers and is in the stable flocculent state is equal to the potential energy value of the minimum point on its potential energy curve. Because the degree of the neighboring polymer layer intrusion depends on its densities, i.e., the amount of absorbed polymer, the smaller its densities, the greater the intrusion, and so the smaller the minimum interval between two cement particle surfaces. In this case, as can be seen from Fig. 2, the potential energy curve of the mixing term falls toward the lower left-hand side [(a) →(b)] and, thus, the intercement potential energy curve and its minimum point accordingly shift toward the lower left-hand side [(i)→(ii)].

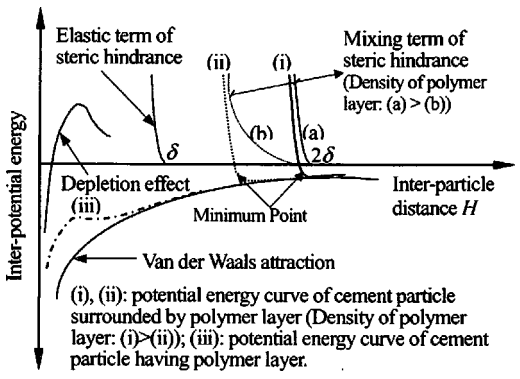

Fig. 2. Interpotential energy of cement particle

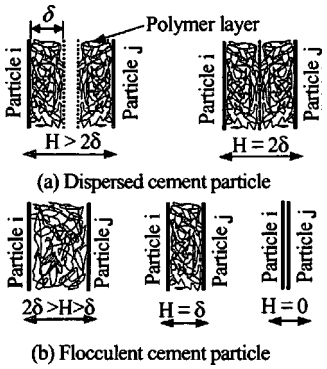

Fig. 3. Dispersed cement particle and flocculent cement particle

However, cement particles that do not absorb the polymer or weakly absorb it will come close and stably flocculate at the surface of the particles due to the depletion effect of free polymers and van der Waals attraction. Thus, the intercement particle potential energy curve is indicated by curve (iii) in Fig. 2. In this study, cement particles, that are more than two times the polymer adsorption layer thickness from the others, are referred to as dispersed cement particles, while the rest are called flocculent cement particles, as shown in Fig. 3. Owing to polymer steric hindrance, flocculent cement particles between 0 and 2δ from each other are near each other but their surfaces actually are not in contact.

According to the intercement particle potential energy curve shown in Fig. 2, the potential energy of the dispersed cement particles, or the flocculent cement particles, is attractive energy. Thus, if expressing the mean potential energy of cement particles in a flocculent state and dispersed state as E_f and E_d, respectively, the mean potential energy E of all the cement particles is expressed by

$$E = \frac{N_{cf}E_f + N_{cd}E_d}{N_c} = E_f - (E_f - E_d) \cdot \frac{N_{cd}}{N_c} \tag{4}$$

where N_{cd}, N_{cf} = number of flocculent cement particles and the number of dispersed cement particles per unit dimension, respectively.

Variation of Rheological Constants with Standing Time

Standing-Time Dependence of Apparent Viscosity

When fresh concrete is kept at rest, its fluidity generally declines with the elapsed time of the stationary state. It is reported that this fluidity decline is mainly due to cement hydration and collision flocculation of cement particles resulting from Brownian motion (Hattori 1980; Okada 1994).

When repulsion between cement particles is caused by steric hindrance, the physical flocculation of the cement particles due to Brownian motion is not obstructed by a potential energy barrier as in the case of static–electric repulsion that yields the primary maximum on the interparticle potential energy curve. The de-

J. Mater. Civ. Eng., 2004, 16(3): 247-256

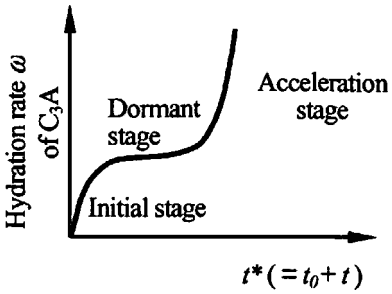

Fig. 4. Variation of hydration rate of C_3A ingredient with time

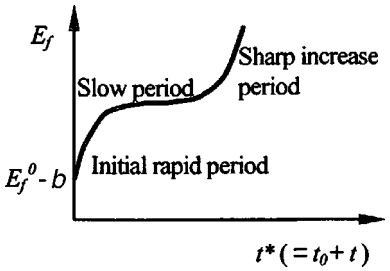

Fig. 5. Assumption on variation of mean potential energy of flocculent cement particles with time

crease rate of dispersed cement particles due to the physical flocculation of a particle is given by (Everett et al. 2000):

$$\frac{dN_{cd}}{dt}=-\frac{8kT\cdot N_{cd}^2}{3\eta} \tag{5}$$

where t = time since the reference point of the investigation on the fluidity variation; and η = viscosity of mixing water.

A chemical cause of fluidity decline is cement hydration, which increases the surface energy of the cement particles and lowers the dispersion effect of the superplasticizer by partly covering the absorbed polymers (Nagataki et al. 1981; Sugamata et al. 1999). When crystal substances of hydration products, such as ettringite, are generated around the cement particles, the solid surface area increases, thus the density of the polymer absorption layer decreases. This causes the interparticle potential energy curve to shift toward the lower left-hand side and the potential energy at the minimum point increases accordingly (Sakai et al. 1996). That is the energy that obstructs the flocculent cement particles from dispersing increases.

In the early stage of cement hydration, the hydration products are mainly ettringite formation from C_3A. As a most general expression, the variation with time of the C_3A hydration rate (ω), as shown in Fig. 4, is expressed by (JCI 1996):

$$[1-(1-\omega)^{1/3}]=s\cdot t^* \tag{6}$$

where s = coefficient describing the hydration rate of C_3A; and t^* = time since cement was mixed with water.

The s in Eq. (6) is determined from environmental temperature (T) and the physical and chemical characteristics of C_3A. If the temperature dependence of s is assumed to follow the Arrhenius law, the relation between s and T is

$$s=s_{20}\cdot\exp\left[B\cdot\left(\frac{1}{293}-\frac{1}{T}\right)\right] \tag{7}$$

where s_{20} = constant describing the hydration rate of C_3A at 20°C; and B = ratio of activation energy of C_3A to gas constant (8.314 J/mol k).

Thus, the energy barrier of the flocculent cement particles, which obstructs them from dispersing, is affected by the amount of ettringite formation, and the variation of the mean value E_f with time can be assumed to be, as shown in Fig. 5, based on the variation of the C_3A hydration rate with time (see Fig. 4):

$$E_f=E_f^0-b[1-s(t_0+t)]^3 \tag{8}$$

where E_f^0 = constant; b = constant related to the amount of C_3A ingredient; (E_f^0-1) = initial energy barrier of the flocculent cement particle when there is no hydrate; and t_0 = reference time point referred to the time since the cement was mixed with water to the start of the time-dependence investigation, and is not less than the concrete mixing time.

When the superplasticizer is overdosed by a rate κ (the ratio of the actual dosage to the saturated absorbing amount), there are some of the polymers yet to be absorbed. When the hydrates form outside of the initially absorbed polymers, the excess unabsorbed polymers gradually absorb. Thus, the density of the polymer absorption layer does not change with time. In this case, the mean energy barrier (E_f) of flocculent cement particle can be kept as its initial value (E_f^0-b) in the saturated absorbing state until a certain time, t_c. From the viewpoint of the change of E_f, this fluidity maintenance effect of the excess polymers is equivalent to a gradual reduction of E_f while the hydrates increase E_f. If assuming that the total reduction in E_f is proportional to the amount of excess polymers and the value of the E_f in the saturated absorbing state, the total reduction in E_f is equal to $(\kappa-1)(E_f^0-b)$, and t_c can be obtained as shown in the notes of Eq. (9) based on Eq. (8). However, when the time lapse is over t_c, the excess polymers are exhausted, and the density of the polymer layer decreases with time due to the increase in the hydrates. As a result, E_f decreases with time. In this case, the E_f-t relation is expressed by the second equation in Eq. (9) according to Eq. (8)

$$E_f=\begin{cases}E_{fs}^0-b & (0\leq t_0+t\leq t_c)\\ E_{fs}^0-[1-s(t_0+t)]^3-(\kappa-1)(E_{fs}^0-b) & (t_c<t_0+t)\end{cases} \tag{9}$$

where $t_c=1/s\cdot[1-\sqrt[3]{1-(\kappa-1)(E_{fs}^0-b)/b}]$.

Integrating Eq. (5) over time t, the number of dispersed cement particles at any time is obtained as

$$\frac{1}{N_{cd}}-\frac{1}{N_{cd0}}=\frac{8kT}{3\eta}\cdot t \tag{10}$$

where N_{cd0} = initial number of dispersed cement particles in the beginning of the investigation. If the initial degree of cement particle dispersion is noted by ψ_0, N_{cd0} is equal to $N_c\psi_0$.

By substituting Eq. (10) and Eq. (8) or (9) and into Eq. (4), the mean potential energy barrier of all cement particles in the standstill state, $E_{ss}(t)$, is given as

$$E_{ss}(t)=E_f-(E_f-E_d)\cdot\frac{\psi_0}{1+8kT\psi_0N_ct/3\eta} \tag{11}$$

where E_d = mean potential energy of dispersed cement particles, and is a constant for a certain specimen.

Eq. (11) shows that the mean potential energy barrier of the cement particles increases with a lapse of standstill time when the polycarboxylate-based superplasticizer is added. Moreover, since the hydrates and the decrease in free mixing water result in an increase in the interfrictional angle, the true yield stress (τ_y) of high fluidity concrete increases with elapsed time. Therefore, according to Eq. (2), the η_a of high fluidity concrete increases with the lapse of standstill time.

J. Mater. Civ. Eng., 2004, 16(3): 247-256

It is hard to confirm and to quantify the variation of the interfrictional angle of fresh concrete with the amount of hydrate. If the variation of true yield stress with standing time is ignored, the apparent viscosity $(\eta_a)_{ss}(t)$ of the high fluidity concrete at any time t is expressed by Eq. (12) according to Eq. (2):

$$(\eta_a)_{ss}(t)=\frac{\tau\cdot\exp(E_{ss}(t)/kT)}{C_1\sinh[C_2(\tau-\tau_y)]} \tag{12}$$

Variation of Bingham Constants with Standstill Time

When the Bingham constants are measured with the two-point workability method as shown in Fig. 1, they are expressed by Eqs. (13) and (14) based on Eq. (1):

$$\eta_b=\frac{\tau_H-\tau_L}{\dot\gamma_H-\dot\gamma_L}=\frac{1}{C_1}\cdot\frac{(\tau_H-\tau_L)\cdot\exp(E/kT)}{\sinh[C_2(\tau_H-\tau_y)]-\sinh[C_2(\tau_L-\tau_y)]} \tag{13}$$

where η_b = plastic viscosity; τ_H and τ_L = shear stress of the highest point and the lowest point, respectively; and $\dot\gamma_H$ and $\dot\gamma_L$ = shear rate of the highest point and the lowest point, respectively.

$$\tau_{yb}=\frac{\tau_L\dot\gamma_H-\tau_H\dot\gamma_L}{\dot\gamma_H-\dot\gamma_L}\cong\tau_y+\frac{E}{C_2kT}+\frac{\dot\gamma_H\ln\dot\gamma_L-\dot\gamma_L\ln\dot\gamma_H}{C_2(\dot\gamma_H-\dot\gamma_L)}+\ln\frac{2}{C_1} \tag{14}$$

where τ_{yb} = Bingham yield stress.

Eqs. (13) and (14) indicate that the η_b or the τ_{yb} of the high fluidity concrete increases with the increase in the mean potential energy barrier (E) of the cement particles and, thus, increases with the lapse of standstill time.

Variation of Apparent Viscosity with Agitation Duration

Apparent Viscosity in Agitated State

When acted on by a shear force, e.g., agitation, some of the flocculent cement particles move and become dispersed cement particles. Fresh concrete is caused to flow by the moving particles in it. The flow rate of high fluidity concrete is dependent on the rate of cement particle movement, and is equal to the product of the number and the mean moving distance (Λ_{cm}) of moving cement particles in unit time (Li 2001). Thus, the number of moving cement particles in unit time, i.e., the occurrence rate ($d\lambda/dt$) of moving cement particles, is the ratio of the shear rate ($\dot\gamma$) of fresh concrete to Λ_{cm}, as shown in Eq. (15)

$$\frac{d\lambda}{dt}=\frac{1}{\Lambda_{cm}}\cdot\frac{d\gamma}{dt}=\frac{1}{\Lambda_{cm}}\cdot\dot\gamma \tag{15}$$

It can be considered that the decreasing rate of flocculent cement particle in an agitated state is proportional to the number (N_{cf}) of remaining flocculent cement particles and the occurrence rate ($d\lambda/dt=\dot\gamma/\Lambda_{cm}$) of moving cement particles. However, to enable integral operations, $\dot\gamma/\Lambda_{cm}$ is replaced by the occurrence rate ($d\lambda_0/dt=\dot\gamma_0/\Lambda_{cm}$) of moving cement particles at the start of the shear force, and this decrease rate is expressed approximately by

$$\left(\frac{dN_{cf}}{dt}\right)_{as}\cong-\frac{\alpha\cdot\dot\gamma_0}{\Lambda_{cm}}\cdot N_{cf} \tag{16}$$

where a = proportional constant; and $\dot\gamma_0$ = shear rate at the start point of shear force.

On the other hand, according to Eq. (5), the increasing rate of the flocculent cement particle due to Brownian motion, is given by

$$\left(\frac{dN_{cf}}{dt}\right)_{as}=\frac{8kT}{3\eta}\cdot(N_c-N_{cf})^2 \tag{17}$$

Therefore, the number of flocculent cement particles versus agitation time is expressed by

$$\frac{dN_{cf}}{dt}=-\frac{\alpha\dot\gamma_0}{\Lambda_{cm}}\cdot N_{cf}+\frac{8kT}{3\eta}\cdot(N_c-N_{cf})^2 \tag{18}$$

By integrating Eq. (18) over time, the number of flocculent cement particles at any time is given by

$$N_{cf}=m_7-\frac{2m_4}{m_5\exp(-m_6\cdot t)+1} \tag{19}$$

where $m_4=3\alpha\eta\dot\gamma_0/16\Lambda_{cm}kT\cdot\sqrt{32kT\Lambda_{cm}N_c/3\eta\alpha\dot\gamma_0+1}$; $m_5=2m_4/(m_4+N_{cd0}+3\alpha\eta\dot\gamma_0/16\Lambda_{cm}kT)-1$; $m_6=16kTm_4/3\eta$; and $m_7=m_4+N_c+3\alpha\eta\dot\gamma_0/16\Lambda_{cm}kT$.

Furthermore, by substituting Eqs. (8) and (19) into Eq. (4), the relation between the mean potential energy barrier $E_{as}(t)$ of all cement particles and time in an agitated state is obtained as

$$E_{as}(t)=E_d+\frac{1}{N_c}\{E_f^0-E_d-b[1-s(t_0+t)]^3\}\times\left[m_7-\frac{2m_4}{m_5\exp(-m_6t)+1}\right] \tag{20}$$

Hence, the shear rate $\dot\gamma(t)$ and the apparent viscosity $(\eta_a)_{as}(t)$, at any agitation time for high fluidity concrete produced by mixing polycarboxylate-based superplasticizer, are calculated by Eq. (21) derived by substituting Eq. (20) into Eqs. (1) and (2)

$$\dot\gamma_t=C_1\exp\left(-\frac{E_{as}}{kT}\right)\cdot\sinh[C_2(\tau-\tau_y)]$$

$$(\eta_a)_{as}(t)=\frac{\tau\cdot\exp(E_{as}/kT)}{C_1\sinh[C_2(\tau-\tau_y)]} \tag{21}$$

Conditions where Apparent Viscosity Varies with Load Duration

Differentiating $E_{as}(t)$ shown in Eq. (20) with respect to t yields:

$$\frac{dE_{as}(t)}{dt}=\frac{3bs[1-s(t_0+t)]^2}{N_c}\cdot\left(m_7-\frac{2m_4}{m_5\exp(-m_6t)+1}\right)-\frac{E_f^0-E_d-[1-b(t_0+t)]^3}{N_c}\cdot\frac{2m_4m_5m_6\exp(-m_6t)}{[m_5\exp(-m_6t)+1]^2} \tag{22}$$

By taking the right-hand side of Eq. (22) to be positive or negative, and carrying out numerical calculations, it is possible to obtain two ranges of initial shear rate $\dot\gamma_0$. When applying the shear stress that can create an initial shear rate falling into any one of the two ranges, the apparent viscosity increases or decreases with agitation time in the initial period of load, two ranges of constant shear stress can be further determined. The elapsed time (t_e) until the apparent viscosity reaches equilibrium under a certain constant shear stress can be also obtained. If the right-hand side of Eq. (22) is taken to be zero, an initial shear rate $\dot\gamma_0$ can be obtained to make the apparent viscosity constant with

J. Mater. Civ. Eng., 2004, 16(3): 247-256

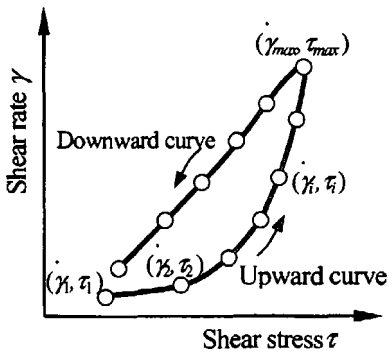

Fig. 6. Hysteresis loop and step-by-step load

agitation time. However, it is hard to express these ranges or values of $\dot{\gamma}_0$ and t_e with equations because they are very complicated.

However, in the event of a superplasticizer overdose, or in the hydration dormant stage, since hydration is slow, the effect of the hydrates on the mean potential energy of the cement particles is small. If this effect is ignored, the differential Eq. (22) can be simplified as

$$\frac{dE_{as}(t)}{dt} \cong -\frac{E_f^0 - E_d}{N_c} \cdot \frac{2m_4 m_5 m_6 \exp(-m_6 t)}{[m_5 \exp(-m_6 t)+1]^2} \tag{23}$$

Taking the right-hand side of Eq. (23) to be positive, a condition expressed by an upper limit of initial shear rate for increasing the apparent viscosity with agitation time is obtained as

$$\dot{\gamma}_0 < \frac{8kT\Lambda_{cm}}{3\alpha\eta} \cdot \frac{N_{cd0}^2}{N_c - N_{cd0}} \tag{24}$$

When the initial shear rate ($\dot{\gamma}_0$) is less than the upper limit shown on the right-hand side of Eq. (24), since the flocculation rate of cement particles is greater than the dispersion rate, even if the shear stress is fixed, the shear rate decreases with shear stress duration, and the apparent viscosity increases until equilibrium is reached.

However, taking the right-hand side of Eq. (23) to be negative, a value expressed by a lower limit of the initial shear rate for making the η_a decrease with agitation time can be obtained as

$$\dot{\gamma}_0 > \frac{8kT\Lambda_{cm}}{3\alpha\eta} \cdot \frac{N_{cd0}^2}{N_c - N_{cd0}} \tag{25}$$

If the initial shear rate ($\dot{\gamma}_0$) is more than the lower limit shown on the right-hand side of Eq. (25), the flocculation rate of cement particles is smaller than the dispersion rate. Thus, the shear rate increases with stress duration when the shear stress is fixed, and the η_a decreases until the equilibrium is reached.

Conditions of Constant Apparent Viscosity

The initial shear rate ($\dot{\gamma}_0$) for maintaining the initial apparent viscosity, i.e., the shear rate necessary to make the apparent viscosity not change with agitation time, can be derived as given by Eq. (26) by taking the value of the right-hand side of Eq. (23) to be zero

$$\dot{\gamma}_0 = \frac{8kT\Lambda_{cm}}{3\alpha\eta} \cdot \frac{N_{cd0}^2}{N_c - N_{cd0}} \tag{26}$$

When the initial shear rate ($\dot{\gamma}_0$) equals the value given by Eq. (26), the flocculation rate of cement particles is equal to the dispersion rate, and both the shear rate and apparent viscosity are maintained at their initial values.

Table 1. Mix Proportions and Consistency of High Fluidity Concrete

Mixture No.	N	K	B
Type of cement	OPC[a]	B-type slag cement	Blite
Water–cement ratio (%)	25	23	25
Sand aggregate (%)	50	50	50
Superplasticizer ($C\times$%)	5.33	4.00	2.82
Unit weight (kg/m^3)			
Water	144	139	149
Cement	576	596	596
Sand	839	817	817
Gravel	839	817	817
Slump (cm)	23.7	28.0	23.0
Slump flow (cm)	51.5	69.5	59.5

[a]OPC: Ordinary Portland cement.

If the hydrate effect is not taken into account, after a certain agitation time, the flocculation of the cement particles resulting from Brownian motion reaches equilibrium with the dispersion caused by the agitation. Once this equilibrium state is reached, the mean potential energy barrier $E_{as}(t)$ does not vary with agitation time. Based on Eq. (20), the mean potential energy barrier E_{as-e} and the apparent viscosity $(\eta_a)_{as-e}$ in the equilibrium state are expressed by

$$E_{as-e} = E_d + (E_f^0 - E_d) \cdot \frac{m_7 - 2m_4}{N_c}$$

$$(\eta_a)_{as-e} = \frac{\tau \cdot \exp(E_{as-e}/kT)}{C_1 \sinh[C_2(\tau - \tau_y)]} \tag{27}$$

The value of $[(m_7-2m_4)/N_c]$ is less than 1, and decreases with the increase in initial shear rate ($\dot{\gamma}_0$). Thus, $(\eta_a)_{as-e}$ decreases with increasing $\dot{\gamma}_0$.

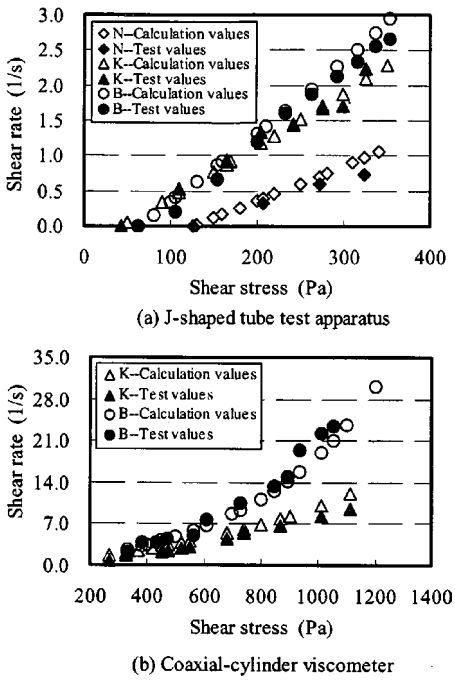

Fig. 7. Comparison of test results and calculation results for flow curve of high fluidity concrete

J. Mater. Civ. Eng., 2004, 16(3): 247-256

Table 2. Setup of Parameter Values in Eq. (1) *for All High Fluidity Concrete Specimens*

Mixture No.	τ_y (Pa)	S_d	T (K)	N_c (10^{11})	Λ_{cm} (10^{-12} m)	E_f (kT)	E_d (kT)	Ψ_0	C_1 (10^{13})	C_2 (10^{-3})
N	126	0.226	293	1.6775	8.0	41	5	0.300	1.6	1.90
K	43.1	0.238	293	1.8891	7.5	41	5	0.315	1.7	1.62
B	62.8	0.238	293	1.6839	10.0	41	5	0.305	2.1	2.42

For a measured apparent viscosity error e (<1), the measured value of $(\eta_a)_{as-e}$ is expressed as

$$[(\eta_a)_{as-e}]_m=(1\pm e)\cdot(\eta_a)_{as-e} \tag{28}$$

where e equals a positive value when apparent viscosity decreases with agitation time, but is negative when apparent viscosity increases.

By substituting the second equations in Eqs. (21) and (27), respectively, into Eq. (28) and solving, the duration (t_e) of agitation until the apparent viscosity reaches equilibrium is obtained as

$$t_e=\frac{1}{m_6}\ln\left\{m_5\cdot\left[\frac{2m_4(E_f^0-E_d)}{N_c kT\ln(1\pm e)}-1\right]\right\} \tag{29}$$

Thixotropic Characteristic

If measuring the relationship between shear stress (τ) and resulted shear rate ($\dot{\gamma}$) of a non-Newtonian liquid, the obtained downward curve caused by stepwise decreasing stresses does not generally retrace the upward curve caused by stepwise increasing stresses, the measured $\dot{\gamma}-\tau$ relational curve is a hysteresis loop as shown in Fig. 6 (Nakagawa and Kobe 1965). The hysteresis loop is a typical manifestation of the thixotropic characteristic of the material, thus the shape and area of the hysteresis loop are always used to evaluate the thixotropic characteristic. Likewise, owing to the breakdown recovery of flocculent structures of cement particles, the shear flow behavior of high fluidity concrete is affected by past stresses (stress history), and a shear rate thixotropy characteristic is shown. In the following, examining the shape and the area surrounded by the hysteresis loop, the thixotropic characteristic of high fluidity concrete is discussed.

According to Eqs. (19) and (20), the mean potential energy barrier of cement particles at each point on the hysteresis loop shown in Fig. 6 is given by

$$\begin{aligned}
E_1&=E_d+\frac{N_{cf1}}{N_c}\cdot E_r\\
E_2&=E_d+\frac{N_{cf2}}{N_c}\{E_r-b[1-s(t_0+\Delta t_1)]^3\}\\
&\vdots\quad\vdots\\
E_i&=E_d+\frac{N_{cfi}}{N_c}\{E_r-[1-b(t_0+\Delta t_1+\Delta t_2+\cdots\Delta t_{i-1})]^3\}\\
&\vdots\quad\vdots
\end{aligned} \tag{30}$$

where $E_r=E_f^0-E_d$; N_{cfi}=number of flocculent cement particles in the beginning of the i time stress; and Δt_i=duration of the i time stress $N_{cf2}=m_{7-1}-2m_4/(m_{5-1}\exp(-m_{6-1}\cdot\Delta t_1)+1)$, $N_{cfi}=m_{7-(i-1)}-2m_{4-(i-1)}/m_{5-(i-1)}\exp(-m_{6-(i-1)}\cdot\Delta t_{(i-1)})+1$, $m_{4-(i-1)}=3\alpha\eta\dot{\gamma}_{0(i-1)}/16\Lambda_{cm}kT\cdot\sqrt{32kT\Lambda_{cm}N_c/3\alpha\eta\dot{\gamma}_{0(i-1)}}+1$, $m_{5-(i-1)}=2m_{4-(i-1)}/(m_4+N_c-N_{cf(i-1)}+3\alpha\eta\dot{\gamma}_{0(i-1)}/16\Lambda_{cm}kT)-1$, $m_{6-(i-1)}=16kTm_{4-(i-1)}/3\eta$, and $m_{7-(i-1)}=N_c+3\alpha\eta\dot{\gamma}_{0(i-1)}/16\Lambda_{cm}kT$.

Therefore, based on Eqs. (1) and (30), the shear rate of each point on the hysteresis loop is derived as

$$\begin{aligned}
\dot{\gamma}_1&=C_1\exp(-E_1/kT)\sinh[C_2(\tau_1-\tau_y)]\\
\dot{\gamma}_2&=C_1\exp(-E_2/kT)\sinh[C_2(\tau_2-\tau_y)]\\
&\vdots\quad\vdots\\
\dot{\gamma}_i&=C_1\exp(-E_i/kT)\sinh[C_2(\tau_i-\tau_y)]\\
&\vdots\quad\vdots
\end{aligned} \tag{31}$$

where τ_i and $\dot{\gamma}_i$=shear stress and instant shear rate when stress τ_i is applied, respectively, to any point on the hysteresis loop.

The factors influencing the shape and surrounding area of the hysteresis loop cannot be intuitively seen from Eq. (31) but, as discussed in the next section, they can be clarified by numerical calculations based on Eq. (31).

Numerical Calculation Example and Discussion

It is necessary to perform experimental investigations to verify the theoretical results discussed above. However, owing to the segregation of the specimen during testing and the lack of an appropriate test apparatus, it is presently impossible to obtain accurate measurements of the rheological behaviors and their variations with time for fresh concrete. Hence, numerical calculations are carried out here to determine the time dependence and thixotropy of the fluidity of high fluidity concrete, based on the theoretical results just presented.

Flow Curve

Yamamoto et al. (1999) measured a flow curve of high fluidity concrete with a J-shaped tube test apparatus in the low shear rate range and with a coaxial-cylinder viscometer in the high shear rate range. The mix proportions of the specimens used and the test results are shown in Table 1 and Fig. 7, respectively.

After the parameter values in the flow curve of Eq. (1) were calculated or assumed on the basis of the mix proportions of the specimens and the references (e.g., Sakai et al. 1996; Li 2001), as shown in Table 2, the shear rates resulting from different shear stresses are calculated using Eq. (1). The calculated results are

Table 3. Values of Additional Parameters Used in Numerical Analyses on Time-Dependence and Thixotropy of the Fluidity for Mixture K

Series	E_f^0 (kT)	E_{fs}^0 (kT)	Ψ_0	s (10^{-2})	B	α (10^{-16})	η (Pa s)	t_0 (min)	Δt (min)	b
K_1	41	38	0.315	3.5	2,000	5.0	1.0×10^{-3}	5	—	1.0
K_2	41	—	0.358	2.5	—	5.0	1.0×10^{-3}	18	2.5	1.0

J. Mater. Civ. Eng., 2004, 16(3): 247-256

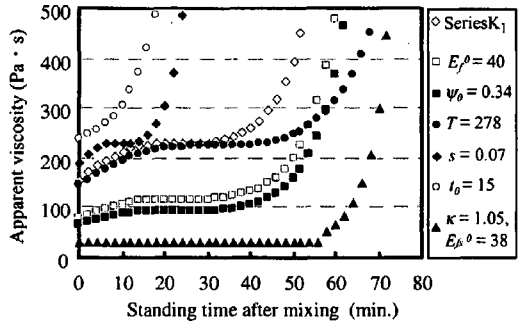

Fig. 8. Effect of standing time after mixing on apparent viscosity of Specimen K

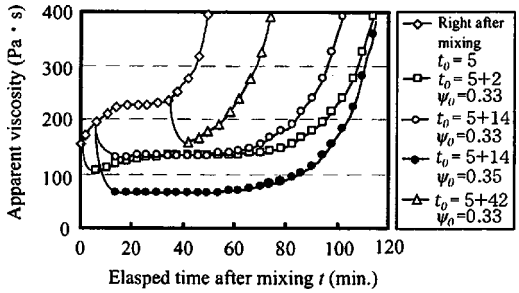

Fig. 9. Effects of agitation at different times on apparent viscosity versus standing time relation curve

shown in Fig. 7 together with the test results. As can seen from Fig. 7, the results are consistent, thus confirming the appropriateness of Eq. (1).

Since the mixture K was used as an object for the numerical analyses on the time dependence and thixotropy characteristic of fluidity, some of the parameters used in these calculations are the same as those used for the flow curve calculation of the mixture K, as shown in Table 2. The values of other necessary parameters are set as shown in Table 3, in which series K_1 is for the numerical analyses of the time dependence of fluidity, and series K_2 is for the thixotropic characteristics. The parameter values in Table 3 are examples set on the basis of the references (Mizukuchi 1984; Yoshino 1996) and trial calculations. The factors influencing time dependence and thixotropy of fluidity are discussed here by changing the settings of parameter values.

Variations of Apparent Viscosity and Bingham Constants with Standstill Time

Fig. 8 shows numerical results of the variation of apparent viscosity (η_a) of the mixture K, whose mixing time was 5 min, with elapsed standstill time (t) under different environmental temperatures and various raw materials or mix proportions. Series K_1 is a normal series, the parameter values used in the calculation of its $\eta_a - t$ relation curve, are listed in Table 2 (series K) and in Table 3 (series K_1) as stated above. As shown in Fig. 8, the η_a of mixture K increases with the standstill time t, but the increasing rate is not a constant, and the $\eta_a - t$ relation curve can be divided into three sections: Initial rapid period, slow period, and sharp increase period. It is considered that the dependence of the increasing rate of η_a on standstill time t results from the variation of the hydration rate of cement with time, the three sections on the $\eta_a - t$ relation curve, respectively correspond to the initial stage, the dormant stage, and the acceleration stage of cement hydration, as shown in Fig. 4.

The differences between the normal series K_1 and the other six series in the parameter values used for the calculation of the $\eta_a - t$ relation curve are shown in the legend of Fig. 8. The different settings in the values of the parameters E_f^0, ψ_0, T, s, t_0, and κ, respectively, mean the change in the superplasticizer dosage, the initial degree of cement particle dispersion, temperature, hydration rate, reference point time, and the overdose rate of superplasticizer. As can be seen from Fig. 8, the reference point time t_0 strongly affects the $\eta_a - t$ relation, and the variation of η_a with standing time is remarkable when t_0 is 15 min, because the cement hydration enters the acceleration stage. Also, the greater the initial dispersion of cement particles ψ_0, the less the increase in η_a with standing time. These results theoretically confirm the observation that the concrete mixing time and the stress history affect the fluidity versus standing time of high fluidity concrete.

Moreover, the increasing rate of η_a with standing time decreases as the superplasticizer dosage is raised. In case of overdosing, the fluidity of the specimen is maintained for a certain period, and the increase in η_a with standing time increases with temperature (T) or the hydration rate (s).

Fig. 9 shows five apparent viscosity versus standing time curves for the mixture K just after the specimen was produced ($t_0 = 5$ min) and agitated at different times ($t_0 = 5 + 2$ min, $5 + 14$ min, and $5 + 42$ min). Here, the effect of the agitation is characterized by the increase in the degree of cement particle dispersion (ψ_0). Higher ψ_0 means that a greater agitation was applied. As shown in Fig. 9, the agitation extends the slow period section on the $\eta_a - t$ relation curve, and postpones the onset of the sharp increase period. These effects also become remarkable when increasing agitation intensity.

Fig. 10 shows the variations of plastic viscosity and Bingham yield stress of mixture K with elapsed standstill time after the specimen is produced and agitated at 42 min after mixing, respectively. The Bingham constants increase with elapsed standstill time, but the increasing rates vary with the hydration stages, and are the greatest in hydration acceleration stage. Furthermore, the agitation can lower the Bingham constants, but does not change the tendencies of the Bingham constants versus standstill time curves following the agitations.

Variation of Apparent Viscosity with Agitation Time

Figs. 11 and 12 show the variation of apparent viscosity of the mixture K with agitation duration for a fixed agitation intensity. The initial shear rates ($\dot{\gamma}_0$) shown in the legends of Figs. 11 and 12 are instant shear rates resulting from each constant agitation at the beginning of agitation, and are thus employed to characterize the intensity of each constant agitation. If considering the effect

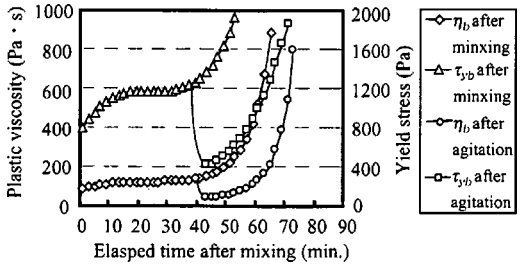

Fig. 10. Variations of Bingham constants with standing time and effects of agitation

J. Mater. Civ. Eng., 2004, 16(3): 247-256

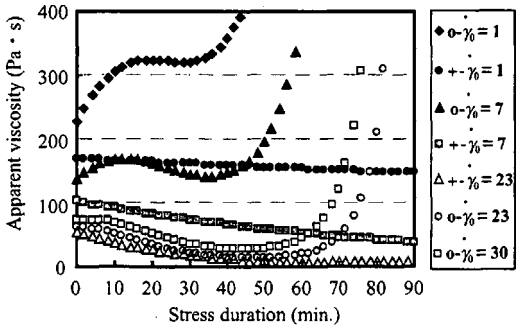

Fig. 11. Variation of apparent viscosity with duration of stress applied (○: The effect of hydrates is taken into account, +: The effect of hydrates is ignored)

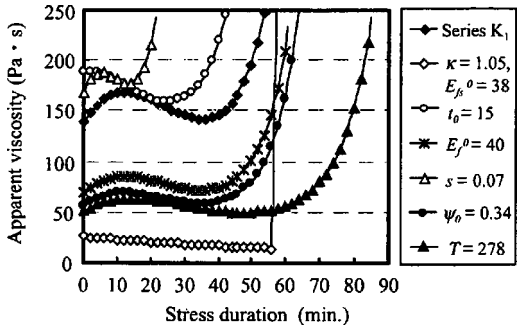

Fig. 13. Effects of various factors on apparent viscosity versus stress duration relation curve when the effect of hydrates is taken into account

of hydration on fluidity versus agitation duration, as can be seen from Fig. 11, the slow period of the $\eta_a - t$ relation curve lengthens, and the η_a in this period decreases with agitation time. However, the η_a still increases with agitation time in the initial rapid period or the sharp increase period, because the hydration is active in these two periods. Once the initial shear rate $\dot{\gamma}_0$ is greater than a certain limit, i.e., an intensive agitation is applied, the η_a decreases with agitation time even in the initial rapid period.

If the effect of the hydration on fluidity versus agitation duration is ignored, and $\dot{\gamma}_0$ is greater than a certain limit, the η_a decreases with agitation time in the initial agitation period, but after a certain elapsed time of agitation (t_e) the η_a obviously approaches a constant, as shown in Figs. 11 and 12. Both the decreasing rate of η_a at the same time point and the time t_e increase with increasing $\dot{\gamma}_0$. However, if $\dot{\gamma}_0$ is smaller than the limit, the η_a increases with the elapsed time of agitation in the initial period. In this case, both the t_e and the rising rate of η_a increase with decreasing $\dot{\gamma}_0$. Moreover, when the applied agitation has a specified intensity, e.g., $\dot{\gamma}_0 = 0.0045$ in this calculation, the η_a does not vary with agitation duration.

Furthermore, the effects of the superplasticizer dosage, initial degree of cement particle dispersion, temperature, hydration rate, reference point time, and superplasticizer overdose rate on the apparent viscosity versus agitation time relation are examined respectively by changing the values of parameters E_f^0, ψ_0, T, s, t_0, and κ, respectively. The numerical results when $\dot{\gamma}_0$ is 7 s^{-1} are shown in Fig. 13. It shows that the η_a decreases with agitation time in the slow period on the apparent viscosity versus agitation time curve. The slow period lengthens with either increasing superplasticizer dosage (i.e., E_f^0 is reduced) or the ψ_0, or decreasing temperature T or the hydration rate s. When the superplasticizer is overdosed, the η_a decreases with agitation time until a certain time. Moreover, Fig. 13 shows that the apparent viscosity versus agitation duration relation curve is affected by the reference point time t_0.

Effect of Stress History on Hysteresis Loop

Fig. 14 shows the calculation results of the hysteresis loop for different stress durations (Δt) when the number of stress steps and the stress magnitude at every step are fixed. The reference point time (t_0) is set to be 18 min, when the cement hydration entered the dormant stage according to a preliminary calculation using Eq. (6). As shown in Fig. 14, when the stress duration (Δt) is less than a certain limit, the downward curve of the $\dot{\gamma} - \tau$ relation curve is above the upward curve. The surrounding area increases with increasing the Δt. However, when the stress duration (Δt) is more than the limit, the latter part of the downcurve is plotted under the upcurve. If the Δt is increased further, the whole downward curve drops below the upward curve, i.e., antithixotropy. This is because great Δt makes the durations of the latter stepwise-decreasing stresses, even all of the descent stresses in the hydration acceleration stage, so that the sharp increases in the hydrate quantities cause a remarkable decrease in the shear rate. The antithixotropy was already observed by Banfill in the experiments of cement paste (Richard et al. 1988).

Fig. 15 shows the effect of the reference point time (t_0) on the hysteresis loop. The area surrounded by the hysteresis loop decreases with increasing t_0 up to a certain limit. If the t_0 is beyond this limit, the downward curve drops under the upward curve, due to the hydration entering the acceleration stage.

Fig. 16 shows the effects of the number of stress steps and the stress magnitude of each step on the hysteresis loop when the duration of each stress is fixed at 2.5 min. The area surrounded by

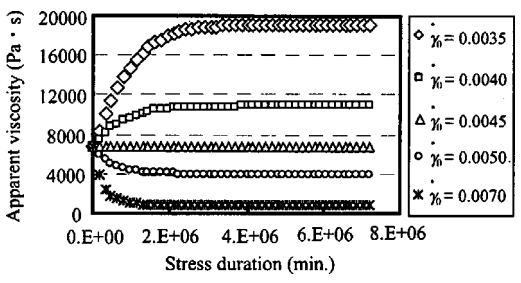

Fig. 12. Relationship between apparent viscosity and stress duration when the effect of hydrates is ignored

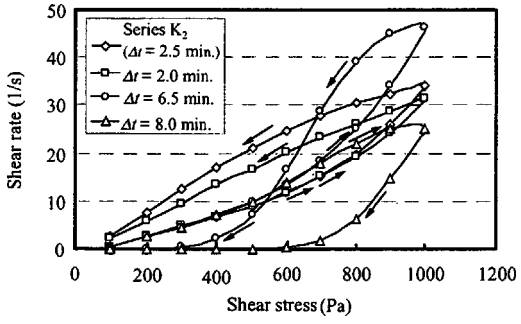

Fig. 14. Effects of stress duration on hysteresis loop of Specimen K

J. Mater. Civ. Eng., 2004, 16(3): 247-256

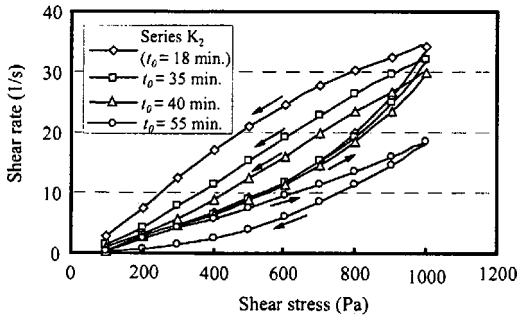

Fig. 15. Variations of shape and surrounded area of hysteresis loop with starting point time of hysteresis loop

a hysteresis loop increases by increasing the number of stress steps when the maximum stress is fixed, or the magnitude of each stress as the number of stress steps is not changed.

Conclusions

In this study, a microscopic approach was first made to the effects of Brownian motion and external shear force on the dispersion degree of cement particles, and the dependence of the intercement particle potential energy on the hydrate generation and the dispersion degree of cement particles. Then, the relationships were quantified between the mean potential energy of the cement particles and various influencing factors, including temperature, superplasticizer dosage, hydration rate of the cement, dispersion degree of cement particles in the starting point of investigation, and elapsed time of stationary state or agitated state. Based on these results, we respectively modeled the apparent viscosity/Bingham constants/shear rate–shear stress–elapsed time relationships that characterize the time dependence of fluidity, and clarified, in theory, the decline of fluidity with the elapsed time of the standstill state, and shear thinning and shear thickening behaviors for high fluidity concrete.

Furthermore, a series of numerical analyses were carried out based on the obtained models, the variations of apparent viscosity or Bingham constants with elapsed time of stationary state or agitated state were discussed under different conditions, such as temperature, hydration rate of the cement, superplasticizer dosage, dispersion degree of cement particles, the dependence of the fluidity on standstill time and stress duration, as well as the influencing factors of the dependence, were quantitatively clarified. Moreover, the hysteresis loops of shear rate–stepwise shear stress relation under different conditions were plotted based on numerical results, then the effects of the elapsed time of cement hydration before applying the first shear stress and the number, peak value, and durations of applied stepwise stresses on the shape and area of resulting hysteresis loop were discussed in detail. Not only the thixotropy of the fluidity of high fluidity concrete but also the antithixotropy were confirmed and clarified, in theory, which signify that the fluidity of high fluidity concrete is stress history dependent.

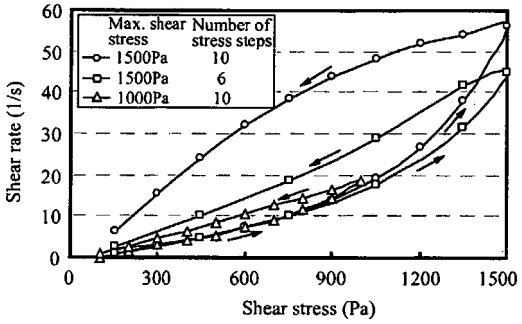

Fig. 16. Effects of magnitude of stress and number of stress steps on hysteresis loop

The numerical models achieved by the microscopic approach in this study can be used to quantitatively predict the fluidity of high fluidity concrete in any time and under any stress state. The obtained numerical results will become a base for accurately evaluating the fluidity of high fluidity concrete, and understanding as well as comparing the differences in fluidity at different times after mixing or after undergoing different stress histories. Further research is needed to develop a test method to accurately measure the variation of the fluidity of the fresh concrete with the elapsed time of standstill state or loading state for verifying the calculation results, and further improving this numerical model.

Notation

The following symbols are used in this paper:

B = ratio of activation energy of C_3A ingredient to gas constant;
$d\lambda/dt$ = rate of cement particle movement;
E = mean potential energy of cement particles;
E_{as-e} = mean potential energy of cement particles in loading state when apparent viscosity becomes a constant;
E_d = mean potential energy of cement particles in dispersed state;
E_f = mean potential energy of cement particles in flocculent state;
E_f^0 = constant, (E_f^0-1) is mean potential energy of cement particles with no hydrate;
E_{fs}^0 = constant, (E_{fs}^0-1) is mean potential energy of cement particles in saturated absorption state of superplasticizer with no hydrate;
N_c = number of cement particles per unit dimension;
N_{cd} = number of dispersed cement particles per unit dimension;
N_{cf} = number of flocculent cement particles per unit dimension;
S_d = stress distribution coefficient;
s = hydration rate constant related to temperature and activation energy of C_3A ingredient;
T = absolute temperature;
t = elapsed time since the start of fluidity variation examination;
t_e = duration since the beginning of stress until apparent viscosity becomes a constant;
t_0 = reference point time referred to as the time interval since mixing cement with water to the start of fluidity variation examination with elapsed time;
t^* = elapsed time since mixing cement with water;
α = proportional constant;
$\dot{\gamma}$ = shear rate;
$\dot{\gamma}_0$ = instantaneous shear rate when shear stress is applied;
Δt = stress duration;

J. Mater. Civ. Eng., 2004, 16(3): 247-256

η = viscosity of mixing water;
η_a = apparent viscosity;
η_b = plastic viscosity;
Λ_{cm} = mean distance of cement particle movement in unit time;
σ_n = normal stress on the shear plane;
τ = shear stress;
τ_y = true yield stress;
τ_{yb} = Bingham yield stress;
ϕ_m = mean interfrictional angle;
Ψ_0 = initial degree of cement particle dispersion; and
ω = hydration rate of C_3A ingredient.

References

Billerg, P., and Osterberg, T., (2001). ''Thixotropy of self-compacting concrete.'' *Proc., 2nd Int. Symposium on Self-Compacting Concrete*, The Univ. of Tokyo, Tokyo, 99–108.

Japan Society of Civil Engineers (JSCE). (1996). ''The technical situation and problems of high fluidity concrete.'' JSCE, Tokyo, 1–39.

Everett, D. H., et al. (2000). *Basic principles of colloid science*, The Royal Society of Chemistry, Kyoto, Japan, 23–27.

Hu, C., and Lefebvre, F. D. (1996). ''The rheology of fresh high-performance concrete.'' *Cem. Concr. Res.*, 26(2), 283–294.

Hattori, K. (1980). ''The mechanism of slump loss and measures.'' *Materials, The Society of Materials Science, Japan*, 29(318), 34–40.

Japan Concrete Institute (JCI). (1993). ''The report of research committee on superplasticized concrete.'' JCI, Tokyo, 1–56.

Japan Concrete Institute (JCI). (1996). ''The report of research committee on hydration numerical model (I).'' JCI, Tokyo, 6–24.

Li, Z. G. (2001). ''Investigation on the shear flow of self-compacting concrete.'' *Proc., 2nd Int. Symposium on Self-Compacting Concrete*. Tokyo, 69–78.

Li, Z. G., Ohkubo, T., Tanigawa, Y., and Mori, H. (2002). ''Theoretical investigation on shear flow of high fluidity concrete.'' *J. Struct. Construct. Eng., Architectural Institute of Japan*, 562, 1–8.

Masuda, Y., et al. (1998). ''Fundamental study on semi-high fluidity concrete. 2: Time-dependence of slump flow, setting time and properties of hardened concrete.'' *Summaries of technical papers of annual meeting*, Architectural Institute of Japan, Tokyo, A-1, 977–978.

Mizuguchi, Y. (1984). ''Fundamental study on flow characteristic of fresh concrete.'' Doctoral thesis, Kyoto Univ., Japan, 66–68.

Nakagawa, T., and Kobe, M. (1965). *Rheology*, The Publishing House of Misuzu, Tokyo, 456–466.

Nagataki, S., et al. (1981). ''Slump loss of fresh concrete using high range water reducing AE agent.'' *Annual Report of Cement Technology*, Japan Cement Association, Tokyo, 35, 210–213.

Okada, E. (1994). ''Slump loss and application of flowing concrete.'' *Cement & concrete chemistry and application*, Japan Cement Association, Tokyo, 141–147.

Richard, S., and Peter, E. C. (1988). ''The rheological behavior of fresh cement pastes.'' *Cem. Concr. Res.*, 18, 327–341.

Sakai, E., and Daimon, E. (1996). ''The dispersion mechanisms of high range water reducing AE agent/calculation of inter-particle potential energy.'' *Cement and concrete*, Japan Cement Association, Tokyo, 595, 13–22.

Sugamata, T., et al. (1999). ''A study on the particle dispersing effect of polycarboxylate-based superplasticizer.'' *Proc., Japan Concrete Institute*, 21(2), 91–96.

Toussaint, F., Juge, C., Laye, J. M., and Pellerin, B. (2001). ''Assessment of thixotropic behavior of self-compacting microconcrete.'' *Proc., 2nd Int. Symposium on Self-compacting Concrete*, Tokyo, 89–98.

Yoshino, A., et al. (1996). ''Viscosity estimation of high fluidity concrete.'' *Proc., Symposium on Fluidity and Workability of Fresh Concrete*, Japan Concrete Institute, 13–18.

Yamamoto, Y., Homa, A., and Kitsutaka, Y. (1999). ''Study on the fluidity, placement ability and properties of high fluidity concrete.'' *J. Struct. Construct. Eng., Architectural Institute of Japan, Tokyo*, 523, 25–31.

J. Mater. Civ. Eng., 2004, 16(3): 247-256